A Low Frequency Ultra-Wideband Electrically Small Monopole Antenna for HF/VHF Application

Yinfeng Xia [1], Wei Xue [1], Yingsong Li [1,2,*], Wanlu Shi [1], Beiming Li [1]

[1] College of Information and Communication Engineering
Harbin Engineering University, Harbin, Heilongjiang 150001, China
*liyingsong@ieee.org

[2] Key Laboratory of Microwave Remote Sensing, National Space Science Center
Chinese Academy of Sciences, Beijing 100190, China

Abstract ─ In this paper, a low frequency ultra-wideband electrically small monopole antenna (ESMA) with a non-foster circuit (NFC) loading for HF/VHF application is proposed. The devised ESMA has a very small height of 30 cm at 18 MHz, whose performance is severely limited due to the electrically small size characterized by large reactance and small radiation resistance. To conquer the limitation of the passive matching method, a NFC is developed and properly designed to cancel out the large reactance of ESMA and broaden the bandwidth. In this paper, the design principle is presented in detail for devising an ESMA system. At last, circuit and electromagnetism co-simulation is constructed to make the results more accurate and convinced. The simulated and measured results indicate that a -10 dB fractional bandwidth of 169% ranging from 18 MHz to 218 MHz is obtained for the designed ESMA matched by the NFC.

Keywords ─ Electrically small monopole antenna, non-foster circuit, ultra-bandwidth.

I. INTRODUCTION

High frequency (HF) band (3-30 MHz) and very high frequency (VHF) band (30-300 MHz) are very popular for radio frequency communications due to their long wavelength, which is appropriate for long-range wireless communications including long-range military communication, frequency modulation (FM) broadcasting, amateur radio, and so on. As an intrinsic and essential component in wireless communication systems, antennas usually exist with the form of large size and perform narrow bandwidth for HF/VHF band applications, which are not always feasible choice. Hence, electrically small antennas (ESAs) are developed for HF and VHF applications owing to their advantage of small electrically size. However, the previously designed ESAs have high-Q impedances characterized by large reactance and small radiation resistance [1-3], which make them difficult to match together. Generally, the passive matching method is the first choice to match the ESAs. Nevertheless, these ESAs matched by the passive matching networks usually lead to a narrow operation band [4].

As is known to us, the non-foster element means the Foster reactance theorem is violated. For example, the element can be designed to provide a negative capacitor or inductor characteristic. In this regard, the non-foster element enables to cancel the high-Q impedance in ESA designs, which of course, can broaden its bandwidth. The first NFC, constructed via negative impedance converters (NICs), was devised and tested by Linviill in 1953 [5]. After that, many NFCs have been utilized to match ESAs. However, most of them are developed based on simulation analyses with ideal models [6-13]. Several early reports have verified the performance of NFC matched ESAs by experimental investigations [14-17]. Theoretically, ESAs matched by NFC can get a very wide frequency band. However, so far, only a few references have reported the achievement of wideband ESAs matched using NFCs [18-20]. Unfortunately, most of them are operated over 30 MHz, while lower frequency band is lack of consideration.

In this paper, a 30-cm ESMA is designed for HF/VHF bands. To enhance its bandwidth, a conventional passive network is utilized to match the ESMA, which leads to a narrow bandwidth. To overcome the limitation of the passive matching method, a floating NFC is developed based on the concept in [21], where the stability of the floating NFC is analyzed and demonstrated. The design procedure of the NFC matched ESMA is given in this paper. To increase the experimental accuracy, the layout of the designed NFC has been analyzed in HFSS and a co-simulation between circuits and electromagnetic is accomplished. The simulated and measured results indicate that a -10 dB fractional bandwidth of 169% ranging from 18 MHz to 218 MHz is achieved for the NFC matched ESMA. And the measured results are in agreement with the simulation ones.

II. ANALYSIS OF THE ELECTRICALLY SMALL MONOPOLE ANTENNA

In this paper, an ESMA that consists of a hollow aluminum conductor, a brass ground plane and a probe-fed with N-type connector is devised. The ESMA has a height of H1=300 mm and a radius of 20 mm, which is installed on a FR4 substrate with a thickness of 2 mm and a size of L×W=200×160 mm². A brass ground plane is printed under the FR4 substrate with the same size, which is designed to meet the requirement of the platform in our project empirically. The antenna model is implemented and analyzed in the HFSS. In addition, a hollow cylinder with the height of H2=240 mm and a radius of 10 mm is also removed from inside of the ESMA to lighten its weight and make it easy to install. The model of the ESMA is presented in Fig. 1
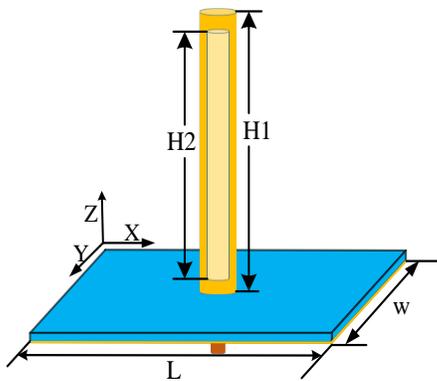
Fig. 1. The geometry of the designed ESMA.

The designed ESMA is simulated and optimized based on the HFSS. To verify the performance of the simulated ESMA, the proposed antenna is also fabricated and measured. The comparison of the simulated and measured reflection coefficients (S11s), real part, imaginary part of input impedance are demonstrated in Figs. 2, 3, and 4, where the measured results are obtained by utilizing the Keysight ENA Series Network Analyzer E5061B.

In Fig. 2, we can see that the antenna is not matched with 50 Ω, and the real is very small given in Fig. 3. From Fig. 4, the simulated imaginary part of the proposed antenna is consistent with the measured result. While there is a little discrepancy between the simulated real part, reflection coefficients and the measured results, which may be caused by the fabrication error and the soldering in the experiments. Anyhow, the simulated and measured input impedance imply that the devised ESMA like other ESAs is still characterized by large reactance and small radiation resistance as observed in Fig. 3 and Fig. 4, which will lead to the mismatch for the ESMA as shown in Fig. 2. Thus, extra effort is needed to increase the bandwidth of the ESMA.
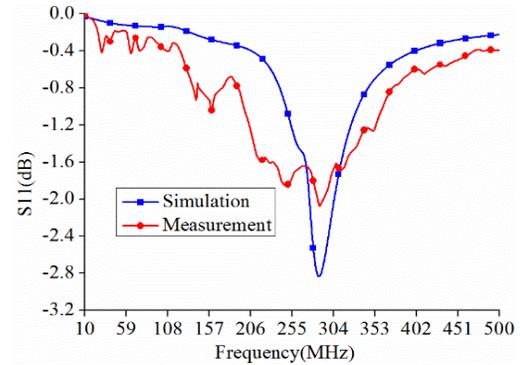
Fig. 2. The reflection coefficients of the ESMA.
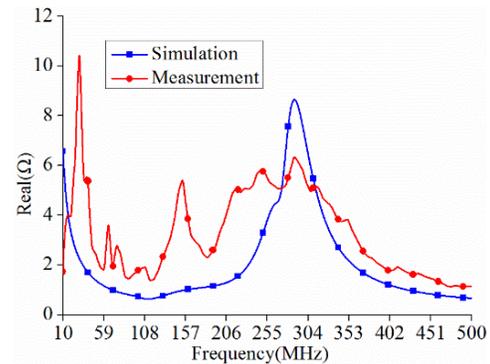
Fig. 3. The real part of the ESMA.
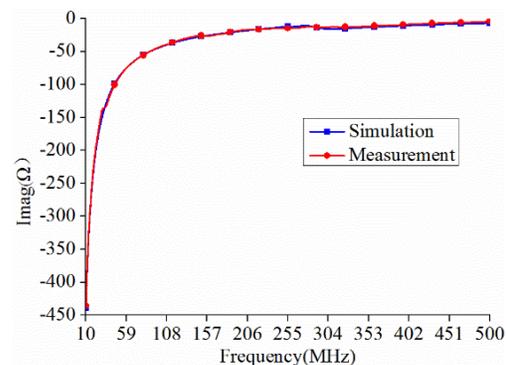
Fig. 4. The imaginary part of the ESMA.

Generally, conventional matching method to broaden the bandwidth of the ESAs is to employ a passive matching network that is composed of some inductors and capacitances in parallel. Like other ESAs, the devised ESMA matched by the passive matching network is presented in Fig. 5, where an inductor and capacitance are utilized, and the simulated S-parameter file of the ESMA is exported into the circuit. Different optimized values of C and L are set to get different operating bandwidth. The results are shown in Fig. 6 and Table 1.
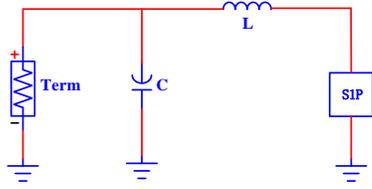
Fig. 5. The schematic of passive matching for the ESMA.

Table 1: The results of different cases

	C (pF)	L (nH)	Frequency Band (MHz)	Fractional Bandwidth
Case 1	324	313	49.7-50.1	0.8%
Case 2	222	80	99.5-100.5	1%
Case 3	138	37	148.7-151.4	1.8%
Case 4	91	22	196.9-202.1	2.6%

From Fig. 6 and Table 1, it can be concluded that the ESMAs matched by four different passive matching networks all have a fairly narrow fractional bandwidth. Moreover, the fractional bandwidth decreases with the operating center frequency shifting toward lower frequency, which means that the lower the frequency band is, the more difficult it is for the ESMA to be matched by using passive matching network. This circumstance can be explained by [2, 3, 22]:

$$B_v = \frac{1}{\eta} \frac{1}{Q} \frac{VSWR-1}{\sqrt{VSWR}}, \qquad (1)$$

$$Q = \frac{1}{ka} + \frac{1}{(ka)^3}, \qquad (2)$$

where Q is the quality factor, k is the wavenumber ($2\pi/\lambda$), a is the radius of the smallest sphere enclosing the entire antenna system, η is the radiation efficiency, VSWR is the voltage standing wave radio, B_v is the fractional bandwidth of the antenna, respectively. According to (1) and (2), B_v is inversely proportional to Q, while Q is inversely proportional to k. Thus, B_v is proportional to the frequency, which implies that the passive network matched ESMA will lead to narrow bandwidth especially at lower frequency band. To overcome the limitation of the passive matching method, a floating NFC is developed to enhance the bandwidth of the ESMA in this paper.

III. NON-FOSTER CIRCUIT MATCHING FOR THE DESIGNED MONOPOLE ANTENNA

In this section, a floating NFC is utilized to match the ESMA. The basic model of a floating NFC is shown in Fig. 7, where port 2 is terminated with the device to be matched by adjusting the load Za, and port 1 is connected with a 50-ohm transmission line. The floating NFC is functioned as a negative inductor or capacitance, which is determined by the impedance of Za.

To choose the proper value of Za, an ideal matching circuit consisting of two ideal elements is constructed to offset the reactance of the ESMA as is demonstrated in Fig. 8. The simulation result is given in Fig. 9, where the major imaginary part of the ESMA is canceled by using the ideal circuit from 10 MHz to 300 MHz. The negative capacitance and negative inductor are -36 pF and -3 nH, respectively.
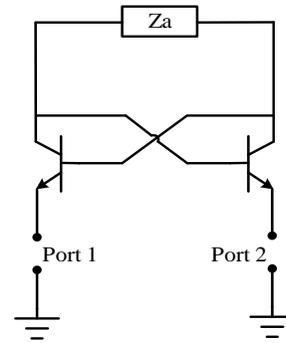
Fig. 7. The model of a floating NFC.

Fig. 6. The reflection coefficients of the passive network matched ESMA.
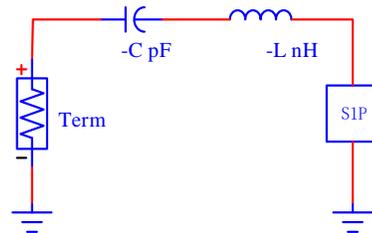
Fig. 8. Ideal matching circuit for the ESMA.
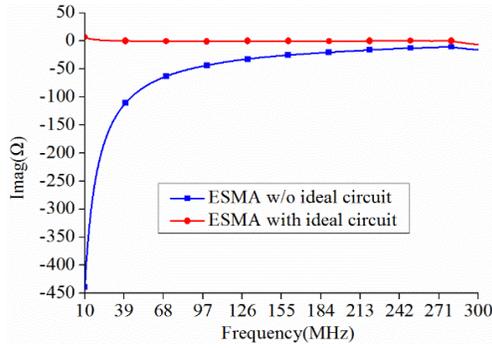
Fig. 9. The imaginary part of the ESMA with/without ideal circuit.

According to the basic model, a floating NFC is built in Fig. 10, where C_block is set to block DC signal and Lb is used to keep the AC signal from disturbing of the DC bias circuit that consists of Rb1, Re1, DC_V1 and Rb2, Re2, DC_V2. The BJT1 and the BJT2 are implemented by NE85633_19960601. The C_load and L_load are employed to cancel the imaginary part of the ESMA, whose values are based on the results of the ideal circuit presented in Fig. 8. To decrease the loss of the NFC, the R_load can be properly adjusted. The simulated results are shown in Fig. 11.
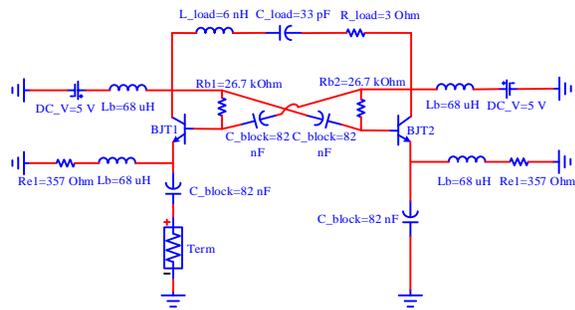
Fig. 10. The designed non-foster circuit.
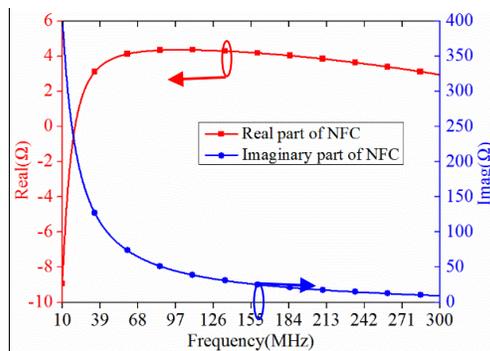
Fig. 11. The input impedance of the designed NFC.

From Fig. 11, the real part of the input impedance is greater than 0 Ω and less than 5 Ω from 20 MHz to 300

MHz, which can guarantee the stability and small loss of the designed NFC in the operating band. The imaginary part of the input impedance acts as the characteristic of a negative capacitance. According to the formula (3):

$$C = -\frac{1}{2\pi \cdot freq \cdot imag(Zin)} \times 10^{12}(pF), \qquad (3)$$

where $imag(Zin)$ is the imaginary part of input impedance, the equivalent negative capacitance of the NFC and ideal circuit can be calculated, which is shown in Fig. 12. By comparing the two lines, it is found that the equivalent capacitance of the NFC is in agreement with that of the ideal circuit. In other words, the designed NFC with small loss and good stability is quite good for matching the ESMA.
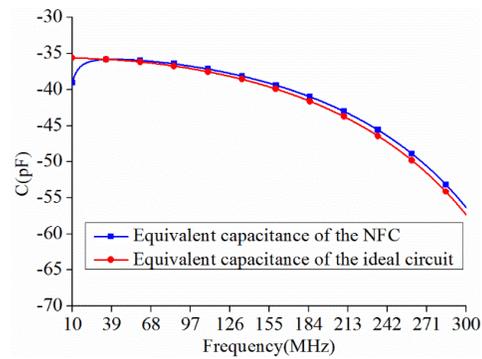
Fig. 12. Equivalent negative capacitance of the designed NFC and ideal circuit.

Based on the former simulation analyses, the entire antenna system is constructed in Fig. 13, where term 1 is connected with a 50-ohm transmission line and the input impedance of the designed ESMA is exported into the term 2 functioning as the ESMA. The NFC, as designed in Fig. 10, is utilized to cancel the large reactance of the ESMA. In addition, a Balun balance-unbalance transformer is employed, which is set to make the real part of the ESMA match to the 50 Ω connector. The simulated results are presented in Fig. 14.
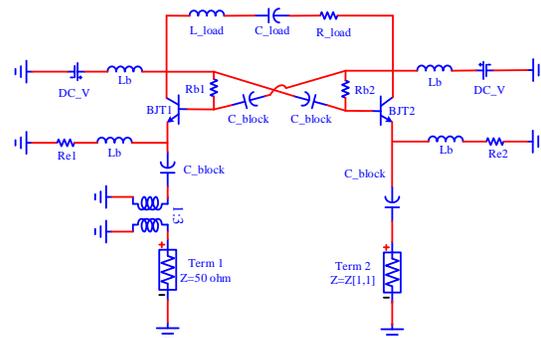
Fig. 13. The schematic of the entire antenna system.
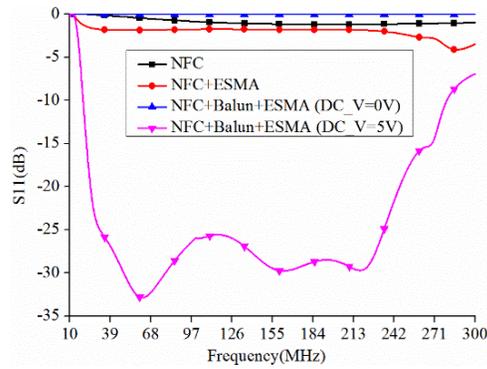
Fig. 14. S11 of the matched and unmatched ESMA.

Figure 14 compares the reflection coefficients of the NFC, the NFC matched to ESMA, and the NFC matched to ESMA with Balun when the voltage resource DC_V turns off/on. It is found that a wide bandwidth can be achieved only when the ESMA is matched by the designed NFC with Balun and DC_V turns on. The obtained wide bandwidth ranges from 20 MHz to 280 MHz, which provides a fractional bandwidth of 173%. The results also demonstrate that this matching method for the ESMA is certainly more effective than the passive matching, especially at lower operating band.

In fact, the NFC is a particularly sensitive circuit, whose performance may be greatly influenced by the parasitic of the circuit layout. To get more precise simulation results, the layout of the designed NFC is modeled and simulated in the HFSS which is shown in Fig. 15, where the lumped ports are utilized to connect the active and passive components. The simulated S-parameter model of the layout is exported into the ADS to construct the co-simulation environment. The results are given, which aims to give a better guidance for the fabrication of the NFC.

(a) Top view   (b) Side view
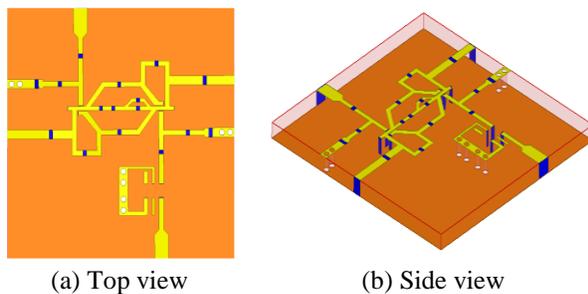
Fig. 15. The layout of the devised NFC.

To verify the simulation results, the antenna system including the ESMA and the designed NFC is fabricated, which is presented in Fig. 16. All the results are shown in Fig. 17.

From Fig. 17, it can be found that the designed NFC matched ESMA will be mismatched when the simulated layout model is exported into the co-simulation without optimization. It is implied that the layout has great impact on the performance of the designed antenna system. At last, we optimize the values of C_load (35 pF) and L_load (22 nH) to eliminate the effect of the layout, and then, a -10 dB fractional bandwidth of 169% ranging from 18 MHz to 218 MHz is obtained and verified by the experiment. The measured return loss is almost in agreement with the simulated result. There is some difference at lower bands, which may be caused by the fabrication error, the soldering and the parasitic effects of the electronic components.

To better understand the principle of the NFC matching of the ESMA, the measured input impedance of the entire antenna system is presented in Fig. 18. From Fig. 18, the imaginary part of the input impedance is about 0 Ω from 18 MHz to 218 MHz, which indicates the reactance of the ESMA has been well canceled by the designed NFC. The real part of the input impedance is about 50 Ω from 18 MHz to 218 MHz, which means that the entire antenna system has been matched to a 50 Ω connector.
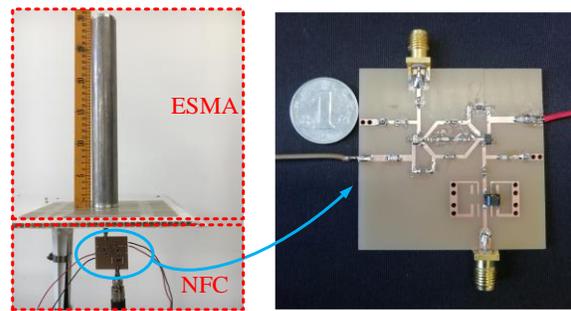
Fig. 16. The fabricated antenna system.
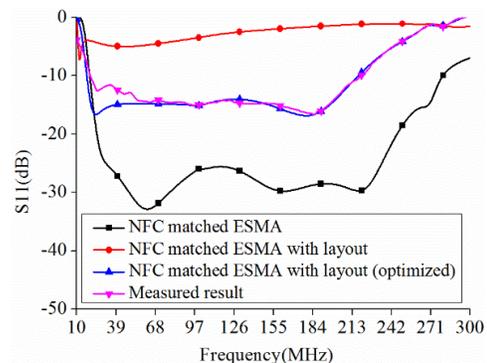
Fig. 17. Simulated and measured return loss.
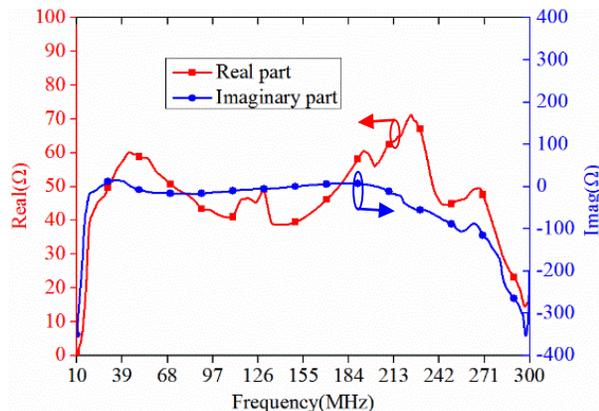
Fig. 18. The measured input impedance of the entire antenna system.

At last, the gain measurement of the fabricated NFC matched ESMA is constructed on a professional test ground, which is shown in Fig. 19. In the process of the measurement, three-antenna method is utilized, which is a popular method for the measurement of this frequency band. The measured results are presented in Fig. 20.

Fig. 19. The measurement setup of the NFC matched ESMA.
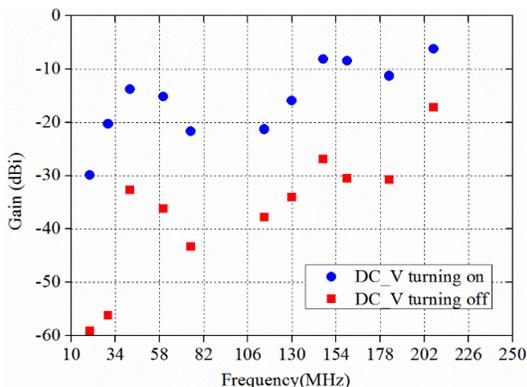
Fig. 20. The measured gain of the NFC matched ESMA.

From Fig. 20, it can be concluded that the gain is improved by about 10 dB when the DC_V turning on in comparison with that the DC_V is off. The results demonstrate that the gain of the ESMA matched by the NFC can be greatly enhanced especially at low frequency band. Moreover, the maximum gain reaches to -6.2 dBi at 207 MHz, which is a good result for the ESMA.

IV. CONCLUSION

In this paper, a 30-cm electrically small monopole antenna is designed for the HF/VHF bands. A non-foster circuit is developed to match the electrically small monopole antenna, which has been conformed to be more effective than the conventional passive matching method. Besides, the design procedure is presented in detail, and an electromagnetic and circuit co-simulation is presented to guarantee the experimental accuracy. The simulation results also verify the great effect of the layout on the performance of entire antenna system. Finally, a -10 dB fractional bandwidth of 169% is obtained, which is also proved by the measured result. In the future, the proposed technique can be used for active metamaterial developments [23] and integrated into the wideband MIMO antenna decoupling [24-31].

ACKNOWLEDGMENTS

REFERENCES

[1] H. A. Wheeler, "Fundamental limitations of small antennas," *Proc. IRE*, vol. 35, no. 12, pp. 1479-1484, Dec. 1947.

[2] L. J. Chu, "Physical limitations of omni-directional antennas," *J. Appl. Phys.*, vol. 19, no. 12, pp. 1163-1175, May 1948.

[3] J. S. McLean, "A re-examination of the fundamental limits radiation Q of electrically small antenna," *IEEE Trans. Antennas Propag.*, vol. 44, no. 5, pp. 672-676, May 1996.

[4] R. M. Fano, "Theoretical limitations on the broad-band matching arbitrary impedances," *J. Franklin Inst.*, vol. 249, no. 1, pp. 57-83, 1950.

[5] J. G. Linvill, "Transistor negative impedance converters," *Proc. IRE*, vol. 41, no. 6, pp. 725-729, June 1953.

[6] P. Jin and R. W. Ziolkowski, "Broadband, efficient, electrically small metamaterial-inspired antennas facilitated by active near-field resonant parasitic elements," *IEEE Trans. Antennas Propag.*, vol. 58, no. 2, pp. 318-327, Feb. 2010.

[7] Z. Ning and R. W. Ziolkowski, "Active metamaterial-inspired broadbandwidth, efficient, electrically small antennas," *IEEE Antennas Wireless Propag. Lett.*, vol. 10, pp. 1582-1585, 2011.

[8] M. Barbuto, A. Monti, F. Bilotti, and A. Toscano, "Design of non-foster actively loaded SRR and application in metamaterialinspired components," *IEEE Trans. Antennas Propag.*, vol. 61, no. 3, pp. 1219-1227, Mar. 2013.

[9] M. Tang, T. Shi, and R. W. Ziolkowski, "Electrically small, broadside radiating huygens source antenna augmented with internal non-foster elements to increase its bandwidth," *IEEE Antennas Wireless Propag. Lett.*, vol. 16, pp. 712-715, Aug. 2016.

[10] J. Church, J. C. S. Chieh, L. Xu, J. D. Rockway, and D. Arceo, "UHF electrically small box cage loop antenna with an embedded non-foster load," *IEEE Antennas Wireless Propag. Lett.*, vol. 13, pp. 1329-1332, July 2014.

[11] S. Koulouridis and J. L. Volakis, "Non-foster circuits for small broadband antennas," *2009 IEEE Antennas and Propagation Society International Symposium,* Charleston, South Carolina, USA, July 2009.

[12] Y. Xia, Y. Li, and S. Zhang, "A non-foster matching circuit for an ultra-wideband electrically small antenna," *13th European Conference on Antennas and Propagation*, Krakow, Poland, 2019.

[13] J. T. Aberle, "Two-port representation of an antenna with application to non-foster matching networks," *IEEE Trans. Antennas Propag.*, vol. 56, no. 5, pp. 1218-1222, May 2008.

[14] N. Zhu and R. W. Ziolkowski, "Design and measurements of an electrically small, broad bandwidth, non-Foster circuit-augmented protractor antenna," *Appl. Phys. Lett.*, vol. 101, no. 2, July 2012.

[15] T. Shi, M. Tang, Z. Wu, H. Xu, and R. W. Ziolkowski, "Improved signal-to-noise ratio, bandwidth-enhanced electrically small antenna augmented with internal non-Foster elements," *IEEE Trans. Antennas Propag.*, vol. 67, no. 4, pp. 2763-2768, Jan. 2019.

[16] S. E. Sussman-Fort and R. M. Rudish, "Non-foster impedance matching of electrically-small antenna," *IEEE Trans. Antennas Propag.*, vol. 57, no. 8, pp. 2230-2241, June 2009.

[17] H. Mirzaei and G. V. Eleftheriades, "A resonant printed monopole antenna with an embedded non-foster matching network," *IEEE Trans. Antennas Propag.*, vol. 61, no. 11, pp. 5363-5371, Nov. 2013.

[18] C. R. White, J. S. Colburn, and R. G. Nagele, "A non-foster VHF monopole antenna," *IEEE Antennas Wireless Propag Lett.*, vol. 11, pp. 584-587, June 2012.

[19] Z. Huang, H. Yang, and T. Liu, "Influence analysis of transmission lines on a stable non-foster-loaded electrically small dipole," *Int. J. Antennas Propag.*, vol. 2019, Article ID: 1273574, Jan. 2019.

[20] M. M. Jacob and D. F. Sievenpiper, "Non-foster matched antennas for high-power applications," *IEEE Trans. Antennas Propag.*, vol. 65, no. 9, pp. 4461-4469, Sept. 2017.

[21] A. M. Elfrgani and R. G. Rojas, "Stability of non-Foster circuits for broadband impedance matching of electrically small antennas," *2015 IEEE Radio and Wireless Symposium*, San Diego, CA, USA, June 2015.

[22] A. D. Yaghjian and S. R. Best, "Impedance, bandwidth, and Q of antennas," *IEEE Trans. Antennas Propag.*, vol. 53, no. 4, pp. 1298-1324, Aug. 2005.

[23] Y. Fan, "Research and Design of Non-foster Active Metamaterial," *Ph.D. Thesis*, Queen Mary, University of London, UK, 2013.

[24] S. Luo, Y. Li, Y. Xia, and L. Zhang, "A low mutual coupling antenna array with gain enhancement using metamaterial loading and neutralization line structure," *Applied Computational Electromagnetics Society Journal*, vol. 34, no. 3, pp. 411-418, 2019.

[25] K. Yu, Y. Li, and X. Liu, "Mutual coupling reduction of a MIMO antenna array using 3-D novel meta-material structures," *Applied Computational Electromagnetics Society Journal*, vol. 33, no. 7, pp. 758-763, 2018.

[26] T. Jiang, T. Jiao, Y. Li, and W. Yu, "A low mutual coupling MIMO antenna using periodic multi-layered electromagnetic band gap structures," *Applied Computational Electromagnetics Society Journal*, vol. 33, no. 3, pp. 305-311, 2018.

[27] T. Jiang, T. Jiao, and Y. Li, "Array mutual coupling reduction using L-loading E-shaped electromagnetic band gap structures," *International Journal of Antennas and Propagation*, vol. 2016, Article ID:6731014, pp. 1-9, 2016.

[28] L. Zhao, F. Liu, X. Shen, G. Jing, Y. Cai, and Y. Li, "A high-pass antenna interference cancellation chip for mutual coupling reduction of antennas in contiguous frequency bands," *IEEE Access*, vol. 6, pp. 38097-38105, 2018.

[29] Y. Kong, Y. Li, and W. Yu, "A minimized MIMO-UWB antenna with high isolation and triple band-notched functions," *Frequenz*, vol. 70, no. 11-12, pp. 463-471, 2016.

[30] Y. Li, W. Li, and W. Yu, "A multi-band/UWB

MIMO/diversity antenna with an enhance isolation using radial stub loaded resonator," *Applied Computational Electromagnetics Society Journal*, vol. 28, no. 1, pp. 8-20, 2013.

[31] S. Luo, Y. Li, Y. Xia, G. Yang, L. Sun, and L. Zhao, "Mutual coupling reduction of a dual-band antenna array using dual-frequency metamaterial structure," *Applied Computational Electromagnetics Society Journal*, vol. 34, no. 3, pp. 403-410, 2019.